MLM--3195

DE85 002552

Mound Activities in Chemical and Physical Research: January-June 1984

Issued: October 22, 1984

MOUND
Miamisburg, Ohio 45342

operated by
MONSANTO RESEARCH CORPORATION
a subsidiary of Monsanto Company

for the
U. S. DEPARTMENT OF ENERGY

Contract No. DE-AC04-76-DP00053

Foreword

This report is issued semiannually by Mound. Under the sponsorship of the DOE Division of Basic Energy Sciences, Mound is responsible for research in the physical sciences to further the progress of science and technology in the public interest. This report is submitted by B. R. Kokenge, Director of Nuclear Operations, and R. E. Vallee, Manager of Technology Applications and Development, from contributions prepared by W. M. Rutherford, Science Fellow (Thermal Diffusion); W. L. Taylor, Science Fellow (Gas Dynamics and Cryogenics); G. L. Silver, Science Fellow (Separation Chemistry); C. J. Wiedenheft, Leader, Metal Hydride Research; and from members of the Isotope Separation Section: W. R. Wilkes, Isotope Separation Manager; E. D. Michaels, Leader, Isotope Separation Research and Development.

These reports are not intended to constitute publication in any sense of the word. Final results either will be submitted for publication in regular professional journals or will be published in the form of MLM topical reports.

Previous reports in this series are:

MLM-2450	MLM-2809
MLM-2506	MLM-2884
MLM-2555	MLM-2892
MLM-2590	MLM-2998
MLM-2654	MLM-3072
MLM-2727	MLM-3125
MLM-2756	MLM-3150

Contents

I. Low temperature research

Reaction rates of $D_2 + T_2$

G. T. McConville, D. A. Menke, and R. E. Ellefson

The reaction rate measurements of the $D_2+T_2 \rightarrow 2DT$ system discussed in previous reports [1,2] indicate that a resonant ion-molecule interaction most likely involving an excited state molecule was necessary to explain the results. A set of reactions was proposed for pure tritium and for tritium containing methane, CT_4, impurity. New rate constants for some of the reactions have been found in the literature. Table I-1 gives the reaction equations along with the revised values of the rate constants k_i. Equations (3) and (9) involve reactions with vibrationally excited T_2. In equation (3) $\nu = 4$ is a representative value for model calculations, because ν can run from 1 to 14. Equation (9) is a channel proposed by Chupka, but the value for k_9 is not certain. The channel has an activation energy of about 3 eV. Another branch for this channel is $T_3^3 + T^-$, but the ratio is not known.

Table I-1 - CALCULATION OF ION DENSITIES IN PURE AND IMPURE TRITIUM EQUATIONS FOR STEADY STATE ANALYSIS (PURE T_2)

Equation No.			Reference No.
1	$e_1^- + T_2 \rightarrow T_2^+ + e_1^- + e_3^-$	$k_1 = 5 \times 10^{-8}$	3
2	$e_3^- + T_2 \rightarrow T + T^-$	$k_2 \sim 10^{-20}$	4
3	$e_3^- + T_2^*(\nu = 4) \rightarrow T + T^-$	$k_3 = 2 \times 10^{-8}$	3
4	$T_2^+ + T_2 \rightarrow T_3^+ + T$	$k_4 = 1.2 \times 10^{-9}$	5
5	$T_3^+ + e_3^- \rightarrow T_2 + T$	$k_5 = 5 \times 10^{-9}$	5
6	$T_3^+ + e_3^- \rightarrow T_2^+ + T^-$	$k_6 = 1.8 \times 10^{-8}$	5
7	$T_3^+ + T^- \rightarrow T_2 + T_2$	$k_7 = 2 \times 10^{-7}$	3
8	$T + T + M \rightarrow T_2 + M$	$k_8 = 2 \times 10^{-32}$	6
9a	$T_2 + T_2^* \rightarrow T_3^+ + T + e_3^-$	$k_9 = 2 \times 10^{-11}$	7
9b	$\rightarrow T_3^+ + T^-$		
	ADDITION OF METHANE, CT_4		
10	$T_3^+ + CT_4 \rightarrow CT_5^+ + T$	$k_{10} = 5 \times 10^{-10}$	8
11	$CT_5^+ + T^- \rightarrow CT_4 + T_2$	$k_{11} = 2 \times 10^{-7}$	3
12	$CT_5^+ + e_3^- \rightarrow CT_4 + T$	$k_{12} = 5 \times 10^{-9}$	5

If one assumes reaction (3) is operative but reaction (9) is not, and $CT_4 = 0$, the following steady state results:

$T_2^+)$ $$ne_1T_2K_1 + T_3^+e_3^- k_6 = T_2^+T_2k_4 + T_2^+e_3^- k_5 \quad (13)$$

$e_3^-)$ $$ne_1T_2k_1 = e_3^-[T_2^* k_3 + T_3^+(k_5+k_6) + T_2^+ k_4] \quad (14)$$

$T_3^+)$ $$T_2T_2k_4 = T_3^+[e_3^-(k_5+k_6) + T^- k_7] \quad (15)$$

$T^-)$ $$e_3^-(T_2^* k_3 + T_3^+ k_6) = T^-T_3^+ k_7 \quad (16)$$

Charge neutrality requires

$$T_2^+ + T_3^+ = e_3^- + T^- \quad (17)$$

In reference 1 the lifetime of e_1^-, the energetic decay electron, was overestimated by a factor of 40. Thus, at any time $(e_1^-) = 2.8/cc$, and each electron averages 155 ionizing collisions, giving $ne_1^- = 4.35 \times 10^2/cc$ with $T_2 = 2.7 \times 10^{19}/cc$. Thus

$$T_3^+ = \frac{ne_1^-T_2k_1 + T_3^+e_3^-k_6}{T_2k_4 + e_3^- k_5}$$

$$= \frac{5.9 \times 10^{14} + T_3^+e_3^- 1.8 \times 10^{-8}}{3.2 \times 10^{10} + e_3^- 4 \times 10^{-9}} \quad (18)$$

We shall show $T_2^+ << T_3^+$, so from the $e_3^-)$ equation, $e_3^-T_3^+ = ne_1^-T_2[K_1/(k_4 + k_5)]$. Thus, with $T_2^* = 0$, $T_2^+ = 3.3 \times 10^4/cc$.

$$T_3^+ = \frac{5.9 \times 10^{14}}{e_3^- 5 \times 10^{-9} + T^- 2 \times 10^{-7}}$$

$$= \frac{5.9 \times 10^{23}}{5e_3^- + 200\ T^-} \quad (19)$$

$$e_3^- = \frac{5.9 \times 10^{14}}{T_3^+ 2.3 \times 10^{-8}} = \frac{5.9 \times 10^{23}}{23\ T_3^+} \quad (20)$$

$$T^- = e_3^- \frac{1.8 \times 10^{-8}}{2 \times 10^{-7}} = 0.09\ e_3^- \quad (21)$$

Since $T_2^+ << T_3^+$, $T_3^+ \doteq T^- + e_3^-$ (22)

and $T_2^+ = 3.3 \times 10^4$, $e_3^- = 1.53 \times 10^{11}$ (23)

$T_3^+ = 1.67 \times 10^{11}$, $T^- = 1.4 \times 10^{10}$ (24)

Thus, with no excited state T_2^*, the ratio of e_3^-/T^- is 11 to 1.

Let $X = T_2^*/T_3^+$, then

$$T_3^+ = \frac{59}{e_3^-(5 + 18 + 20X)} \quad (25)$$

$$T_3^+ = e_3^- + T^- = e_3^-(1 + 0.09 + 0.1X) \quad (26)$$

and

$$(T_3^+)^2 = 59 \frac{(1.09 + 0.01X}{(23 + 20X)} \text{ (units of } 10^{11}) \quad (27)$$

Table I-2 shows increasing T_2^* reduces the ratio of e_3^- to T^- through $e_3^- + T_2^*(\nu=4) \rightarrow T + T^-$. Recent measurements

of ion concentrations in H_2 plasmas [9,10] indicate that the H^-/e^- ratio is nearer 1 to 10.

Table I-2 - DEPENDENCE OF ION CONCENTRATIONS ON T_2^*

X	T_3^+	e_3^-	T^-	T_2^*
0	1.67	1.53	0.14	0
0.01	1.66	1.52	0.14	0.016
0.1	1.61	1.47	0.14	0.16
1.0	1.28	1.07	0.21	1.2
10^1	0.74	0.36	0.38	7.0
10^2	0.57	0.05	0.52	57
10^3	0.55	0.005	0.54	550
10^4	0.54	0.0005	0.54	5500

Thus equation (3) of Table I-1 is a likely measure of excited state T_2^* in tritium gas. A good experimental measure of e^- to T^- in tritium gas would be very useful.

Chupka and co-workers indicate that reaction 9 in Table I-1 is also possible in two channels to produce e_3^- or T^- from excited state T_2^* with an activation energy of about 3 eV.

If $T^* > 0$ and one includes reaction (9a), then B represents strength of reaction (9). Let T_3^+, T^-, and e_3^- be in units of 10^{11} particles.

$$T_3^+ = \frac{59 + BT_2^*}{5e_3^- + 200\ T^-} \qquad (28)$$

$$e_3^- = \frac{59 + BT_2^*}{23\ T_3^+ + 20\ T^*} \qquad (29)$$

$$T^- = e_3^- \frac{18\ T_3^+ + 20\ T_2^*}{200\ T_3^+} \qquad (30)$$

T_3^+, e_3^-, T^- increase, all at the same rate, as B increases. If $B = T_2 k_9$, $BT_2^* = 5.4 \times 10^6\ T_2^*$, see Table I-3.

Table I-3 - T_3^+ AS A FUNCTION OF EXCITED STATE T_2

T_2^*	T_3^+ (units of 10^{11})
10^6	2.31
10^9	50.6
5×10^{12}	3580
5×10^{13}	11300

The rate for reaction (9a) given by Chupka may be too large because of the order of $5 \times 10^{12}\ T_2^*$ increases T_3^+ to 3.6×10^{14}/cc. It is not clear from Souers' electrical conductivity measurements [11] in T_2 that the negative ion concentration is that large. His first analysis indicated that the ion density in the case of no conductivity losses was $N = [(dN/dt)/k]^{\frac{1}{2}}$ where $dN/dt = 1.48 \times 10^{13}$/cc and $K = 2 \times 10^{-7}$ cc/ion, giving $N = 8.6 \times 10^9$/cc. The value of k is for the recombination of H_3^+ and e^-; and, based on the analysis using Table I-1, it is not the limiting rate for the reactions. Thus, $N \sim 10^{11}$ or 10^{12}/cc is probable. An experiment to detect excited state T_2^* and T_3^+ using a CARS technique is being started in collaboration with C. J. Kershner of Mound. A determination of the negative charge density and the e^- to T^- ratio in the limit of no losses would be very useful.

The principal impurity in the T_2 is methane, CT_4. We have shown that increasing CT_4 content in the T_2 inhibits the DT reaction. In a previous report [2] the effect of CT_4 was calculated assuming K_{10} was of the order of 10^{-12} cc/molecule/sec in analogy with the $H_3^+ + D_2 \rightarrow H_2^+D + D$ rate [12]. A new measure of this rate [13] shows it to be much faster with $k = 2 \times 10^{-9}$. Accounting for the mass factor in the velocity, produces $k_{10} = 5 \times 10^{-10}$. Using the k values in Table I-1, the following charge densities are found.

$$T_3^+ = \frac{5.9 \times 10^{23}}{5e_3^- + 200\ T^- + 0.5\ CT_4} \tag{31}$$

$$CT_5^+ = \frac{0.5\ CT_4 T_3^+}{5e_3^- + 200\ T^-} \tag{32}$$

$$e_3^- = \frac{5.9 \times 10^{23}}{23\ T_3^+ + 20\ T_2^* + 5\ CT_5^+} \tag{33}$$

$$T^- = \frac{18\ T_3^+ e_3^- + 20\ T_2^* e_3^-}{200\ T_3^+ + 200\ CT_5^+} \tag{34}$$

If we assume $T_2^* = 5 \times 10^{12}$, e_3^- changes very little, and the equations are simplified as follows, using concentration units of 10^{11}.

$$T_3^+ = \frac{11.8}{e_3^- + 40\ T^- + 0.1\ CT_4},$$

$$e_3^- = \frac{11.8}{4.6\ T_3^+ + CT_5^+ + 200} \tag{35}$$

$$CT_5^+ = \frac{0.1\ CT_4 T_3^+}{e_3^- + 40\ T^-},$$

$$T^- = e_3^- \frac{3.6\ T_3^+ + 200}{40\ T_3^+ + 40\ CT_5^+} \tag{36}$$

$$e_3^- = 0.059 \text{ to } 0.058 \text{ as } T_3^+ = 0 \text{ to } 0.56 \tag{37}$$

$$T^-(T^- + 0.059) = 0.059 \frac{(3.6\ T_3^+ + 200)}{40} \tag{38}$$

$$T^- = 0.514 \text{ to } 0.513 \text{ as } T_3^+ = 0 \text{ to } 0.56. \tag{39}$$

Therefore, with $T_2 = 2.7 \times 10^{19}$/cc, increasing the CT_4 concentration decreases T_3^+ as shown in Table I-4.

Table I-4 - DEPENDENCE OF T_3^+ ON CT_4 IMPURITY

CT_4 (ppm)	T_3^+	CT_5^+
0.01	0.563	0.0005
0.1	0.506	0.005
1.0	0.253	0.319
10.0	0.042	0.534
100.0	0.0045	0.571
1000.0	0.00045	0.576

From the charge neutrality condition, $T^- + e_3^- = 0.573 \sim 0.563$ to 0.576 for $T_3^+ + CT_5^+$, which indicates a consistent set of k_is in Table I-1.

The fact that T_3^+ decreases with increasing CT_4 is consistent with the observed decrease in the rate of DT production with increasing CT_4 concentration. The decrease in T_3^+ in Table I-4 is a consequence of the larger value of k_{10}.

The dependence of the DT reaction rate on CT_4 concentration was then measured at 195 K, in the center of the temperature resonance, as shown in Figure I-1. The point (■) represents 100 ppm CT_4 and the point (□) represents <30 ppm CT_4. The three points in between represent 30, 50, and 75% mixtures of the two. The largest rate at 195 K was measured using T_2 just received from the separation system with a CT_4 concentration $\leq$10 ppm as measured by a gas chromatograph. The 100 ppm and <10 ppm CT_4 points determine a line shown in Figure I-2, where $\tau = 1/K$ is plotted against CT_4 concentration. The point (□) then falls at 20 ppm. The three mixtures between 20 and 100 ppm conform well to the straight line. This behavior is consistent with the gas phase calculation of T_3^+ in Table I-3. The cause of the temperature resonance is still being investigated.

In the last report [14], it was shown that the presence of an ∿500 gauss magnetic field increased the reaction rate at 295 K by a factor of two. The mean time for the reaction decreased from 35 to 16 min. A degaussing coil was constructed so that a 500-gauss alternating field could be reduced to zero around the mixing cell. A measurement of the mean time for the reaction after degaussing was 68 min, nearly a factor of two slower

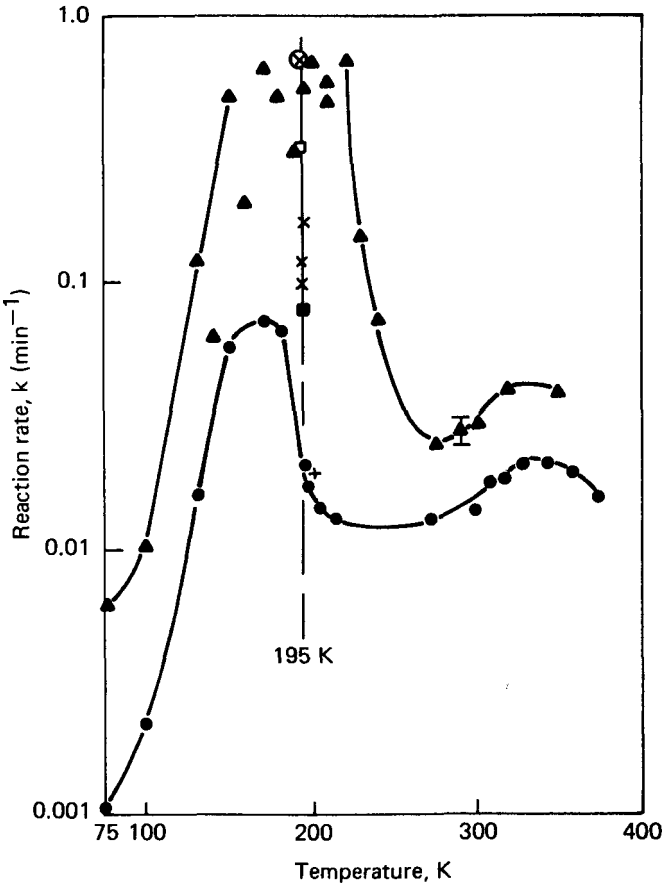

FIGURE I-1 - Concentration dependence of reaction rate, k, on CT_4 impurity at 95 K. ■ = 100 ppm CT_4, □ <30 ppm CT_4, and x <10 ppm new starting T_2.

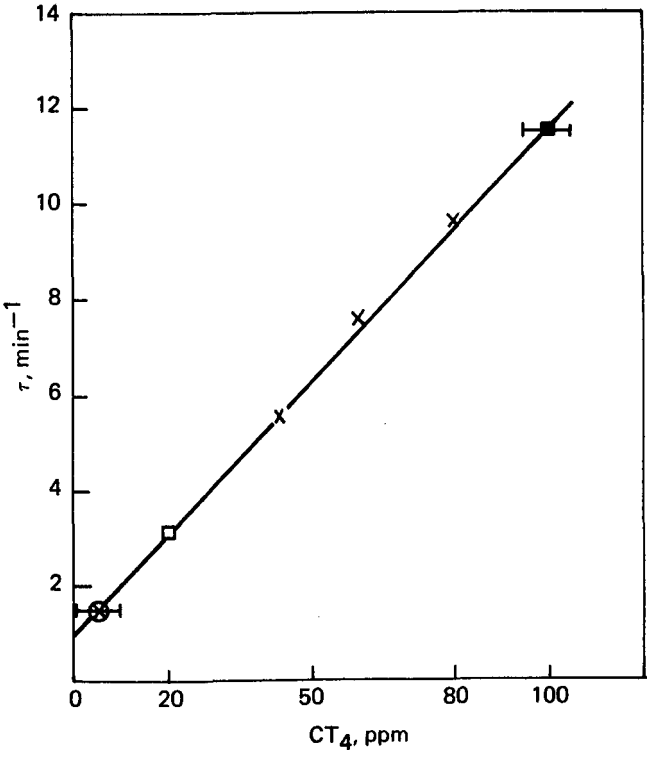

FIGURE I-2 - Dependence of mean time $\tau = 1/K$ on CT_4 concentration. Symbols same as in Figure I-1 (see text).

than the original mean time before the magnetic field was applied to the cell. A possible explanation for this behavior is that the 304 stainless steel loses its nonmagnetic property when the surface is treated to reduce protium ingrowth by removing Fe from the surface. The fact that the reaction was slower after degaussing than the original measurements indicates the original surface must have had a residual field on the surface.

Experiments are under way to try to separate surface effects from gas phase effects in the DT formation rate.

Helium-4 second virial as applied to gas thermometry

G. T. McConville

In the last report [14], it was shown that the agreement between measured and calculated helium-4 second virials can be improved below 10 K by using a helium potential function with a deeper attractive well. The question is how to modify the well without changing the repulsive wall of the potential given in the HFDHE2 potential function. The form and parameters for HFDHE2 were also given in the previous report, where it was shown that, by adding the C_{12} term to the dispersion part of the potential function, the calculation could be brought into agreement with the second virial data of Berry [15]. If we can determine the shape of the potential function near the minimum of the attractive well in an independent way, the calculation of B, the second virial, may be more accurate than the B measured from helium isotherms. The problem is that to determine the nonideality of helium both B and the third virial, C, must be simultaneously extracted from the isotherm. If B can be determined independently, a more accurate measure of C can be found which is important in helium gas thermometry below 10 K.

The HFDHE2 was constructed so that it contained only one undetermined constant, the dispersion parameter D. This parameter was varied to give the best fit to Gammons virials [16] between 100 and 450 K. In the region near room temperature, the data of Briggs [17] are considered to be the most accurate, and they agree with the HFDHE2 calculation to ±0.02 cc/mole. The calculation also agrees with the point at 293 K due to Waxman (NBS) [18] to -0.02 cc/mole. Modifying the low temperature end of the calculation should not make a change in the 293 K agreement.

Now, adding the C_{12} term to the HFDHE2 reduces B at 293 K by 0.05 cc/mole, so a more adequate change needs to be made. The potential form of Feltgren [19] offers a more complicated form. There has been an argument between the German school (Toennes et al.) and the Waterloo school (Scoles et al.) as to whether this increase in complexity of the potential function is necessary. The Feltgren HFIMD function is of the form

$$V(r) = A \exp(-\alpha r-\beta r^2) - \sum_{n=6}^{18} f_n(r) \frac{C_n}{r^n} + B \exp(-br) \quad (1)$$

where

$$f_n = \begin{cases} F_n \text{ for n even} \\ F_n - 1.378 \text{ for n odd} \end{cases}$$

with

$$F_n(r) = P^2(\nu,\alpha r) + (a\alpha r)^m \exp(-1.4\,\alpha r)$$

where

$$P(\nu,\alpha r) = \int_o^{\alpha r} e^{-t} t^{\nu-1} dt/\Gamma(\nu)$$

with $\nu = 1.05\,n + 1.24$

$a = 1.6\,n^{-0.911}$

$m = 1.7\,n - 1.11$

and $\alpha = 8.5 \times [1 + \exp(-a_2 x)]$

where $x = r/r_D$

where r_D is the dispersion length

$$r_D = (C_8 C_6)^{\frac{1}{2}}.$$

The dispersion damping function f_n is very complex. The exponential parameters are the following: A = 222.6 eV, α = -3.807 Å^{-1}, p = -0.1296 Å^{-2}, b = 4.54 Å^{-1} and B is left undetermined. In the damping function a_2 is undetermined. Feltgren et al. [19] measured backward glory scattering to determine a_2 and B, which were given as 1.458 + 0.0055/-0.0027 and 36.4 ± 12 eV. The + numbers represent the inversion of the ^{3}He data and the - numbers the inversion of the ^{4}He data. The calculation of B using the HFIMD form is compared to the HFDHE2 form in Figure I-3. The B from the HFIMD is about 0.3 cc/mole higher than that of the HFDHE2 down to ∿30 K. At lower temperatures they diverge.

Because of the complexity of programming Feltgren's damping function, a series of modifications of the HFDHE2 form was tried to see whether it could be made to fit the low temperature virial data. First, the HFDHE2 damping function was modified using Feltgren's idea [20] that the damping function should depend on the value of n as follows: $f(r_n) = 0.5$ for $r_n = (C_{n+2}/C_n)^{\frac{1}{2}}$ but retaining Ahlrichs' [21] form for f(r):

$$f(r_n) = \exp^{-\frac{D_n}{r}-1} \qquad (2)$$

Thus for n=6, D_6 = 0.818 D; for n=8, D_8 = 0.948 D; and for n=10, D_{10} = 1.123 D. As stated in the previous report [14], this variation in D_n increases the influence of the C_6 term and decreases the influence of the C_{10} term. The quantity D is still an undetermined parameter. Calculations for three values of D are shown in Figure I-3. Curve ① results from D = 1.376 producing ϵ/k = 10.88 K at r_m = 2.964 Å; curve ② results from D = 1.370 producing ϵ/k = 10.92 K at r_m = 2.961 Å; and curve ③ results from D = 1.359 K producing ϵ/k = 11.02 at r_m = 2.957. Curve ② best represents the data. Below 6 K the calculation is significantly higher than the data. Calculation ② produces B = 11.91 cc/mole at T = 293 K, which compares well with the exponential value of 11.89.

A second approach was tried in modifying the exponential repulsion such that A exp($-\alpha_o r$) with α_o = 4.50 Å^{-1} became A exp($-\alpha_1 r - \beta r^2$) where α_1 = 4.49 Å^{-1} and β = 0.01 Å^{-2}. The damping constant D is again independent of n, and a calculation with D = 1.282 is compared with HFDHE2 and the above curve ② in Figure I-4, as shown with the long dash curve. The value of D was chosen to try to fit the data of Berry down to 2.6 K. To fit the lowest temperature data with an HFD form

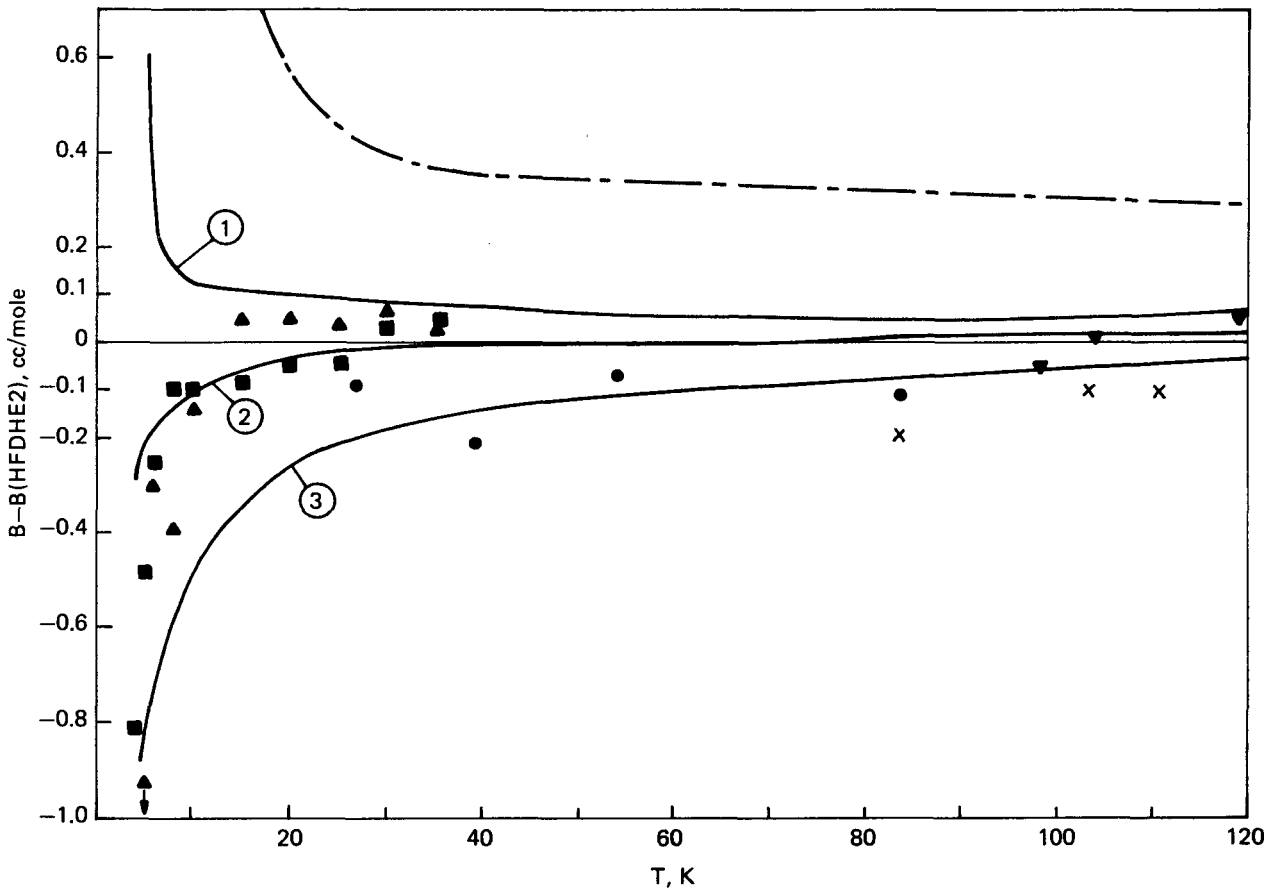

FIGURE I-3 - Comparison of helium-4 second virial data and calculations to HFDHE2 calculation. Data: ■ Berry, ▲ Plumb, ▼ Gammon, ● Kemp, et al. Curves ①, ②, and ③, see text. For data see reference 14.

with a single damping constant, D, produces a curve which is about 0.4 cc/mole below Berry's data at 10 K. At this time a communication was received from Feltgren in which he sent the code to program the incomplete gamma functions in his damping functions and a table of three calculations of B as a function of temperature. The scattering measurements of Feltgren [19] produced different repulsive regions from the inversion of ^{3}He and ^{4}He data. His published potential function represents an average of the two data sets. His B calculated for ^{4}He only is shown as the short dashed curve in Figure I-4. The agreement with Berry's data down to 4 K is very good. This raises an interesting question: Is there a real difference between ^{3}He and ^{4}He in Feltgren's measurements? The answer at the moment is that Feltgren says no. He now feels that the ^{4}He data are better. We may be able to test whether there is an actual difference between the ^{4}He and ^{3}He inversions if the error bars on the ^{3}He second virial data are not too large.

A comparison of the second virial data, taken from Plumb's table [22], to virials calculated down to 2 K is shown on an expanded scale in Figure I-5. Also included in this figure are dielectric constant gas thermometer data of Gugan [23], which we previously thought represented a fit to other existing data. These data are lower than Berry's at

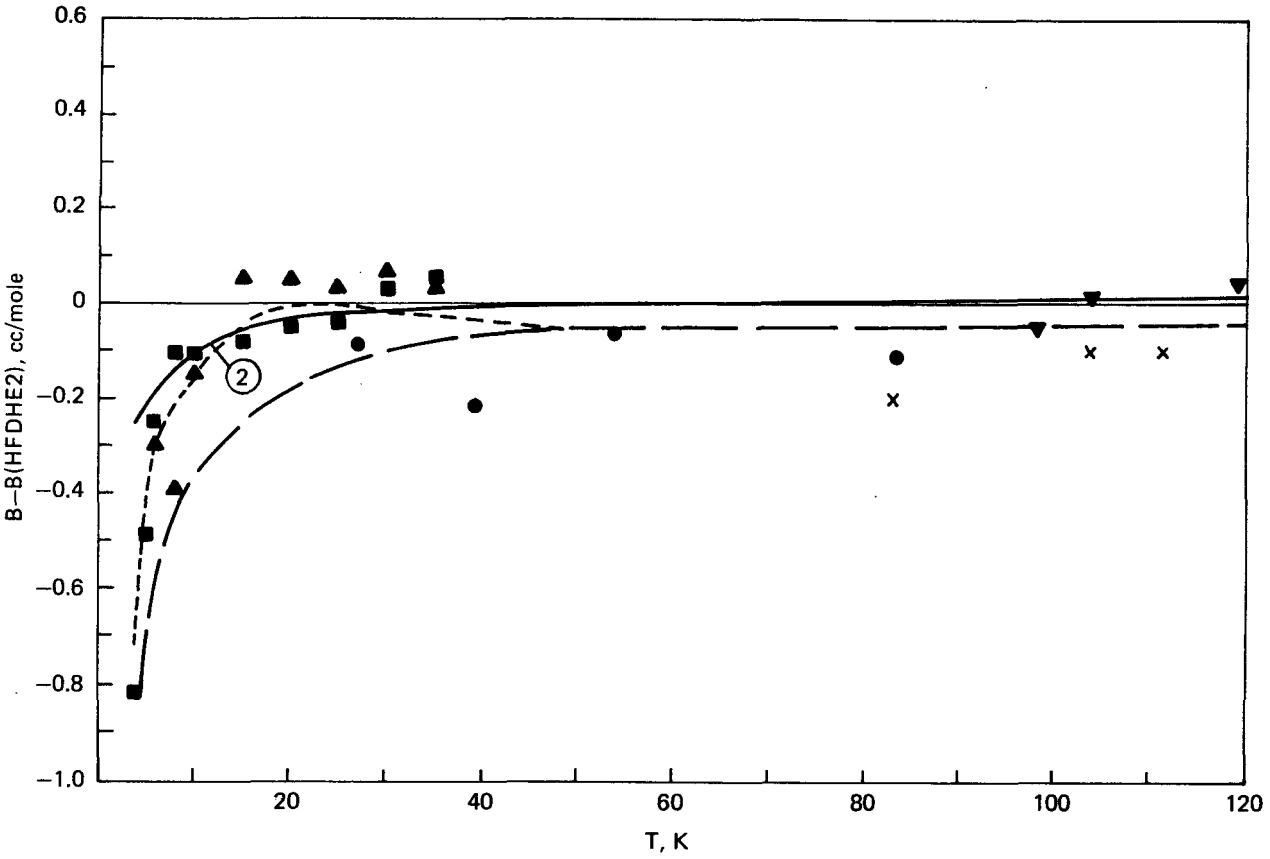

FIGURE I-4 - Comparison of helium-4 second virial calculations to HFDHE2. Data same as in Figure I-3. Curve ② same as in Figure I-3. Calculation --- Feltgren (unpublished) using only ^{4}He inversion of scattering data, -- ---. HFD modified to include exp-βr^2 repulsive term (see text).

temperatures less than 10 K. At 3 K the difference is 0.7 cc/mole. The data plotted as the difference from the HFDHE2 calculation are compared with the three modified potential calculations. The short dashed curve represents Feltgren's calculation. It represents the data very well down to 5 K. Below 5 K the calculation is significantly higher.

Two modifications of the HFDHE2 form shown in Figure I-4 are also shown in Figure I-5. The lower long dashed curve with $\beta = 0.01$ Å^{-2} and D = 1.282 fits the data at the lowest temperatures, but it does not do as well in the region between 5 and 20 K. The case represented by 2 in Figures I-3 and I-4 where $D_6 = 0.818$ D is nearly the same as Feltgren's curve down to 6 K, but then is higher down to 2 K.

The two modifications can be made to converge somewhat by decreasing D slightly (from 1.370 to 1.367) in calculation 2 or by increasing D in the form of HFDHE2 containing β in the repulsive exponent. The shape of curve 2 appears to better represent the low temperature data, indicating that the increase in the influence of the C_6 term (by letting D be a function of n) does produce a better fit to the form of the low temperature data. Two more calculations should confirm this idea.

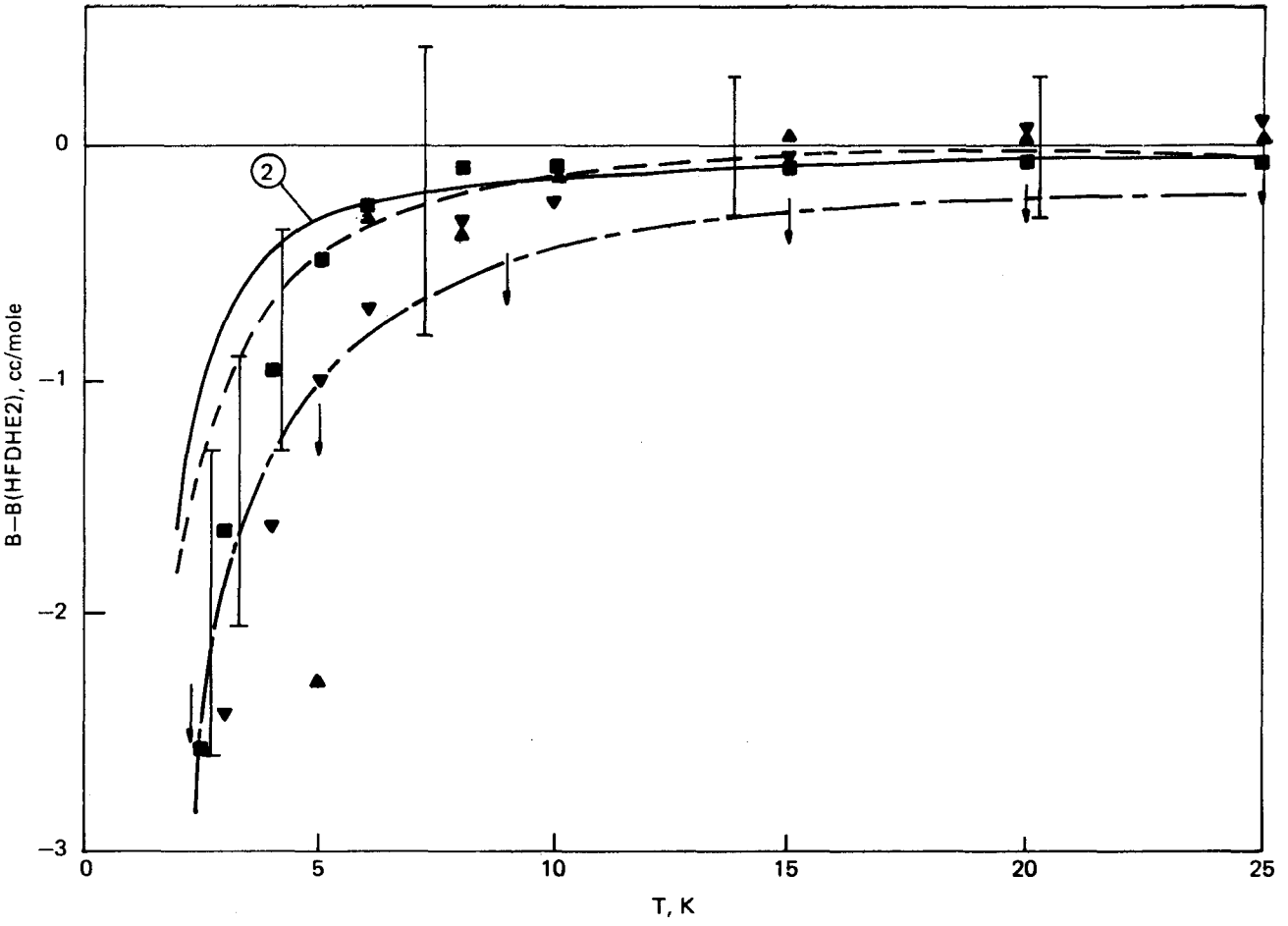

FIGURE I-5 - Comparison of helium-4 second virials on larger scale in the low temperature region. Symbols same as in Figure I-4, except ▼ represents Gugan data. Vertical arrows indicate 1 mK difference from HFDHE2 in gas thermometer with helium density of 1.33 kPa/K.

In terms of temperature uncertainty in a helium gas thermometer operating at a density of 1.33 kPa/K, the vertical arrows in Figure I-5 indicate a difference of 1 mK from the HFDHE2 line. The Feltgren calculation and the modified HFDHE2 using D(n) for n = 6, 8, and 10 agree to better than 0.2 mK between 5 and 25 K. The data below 5 K are about 0.5 mK lower. These calculations show that a well depth of the potential greater than the ab initio well depth of 10.74 K calculated by Liu [24,25] is necessary to fit the improved ^{4}He low temperature second virials. They also show that the detailed shape near the minimum of the well needs to be known to fit the virials below 5 K.

Low temperature trennschaukel

W. L. Taylor

The determination of the thermal diffusion factor of gases using the trennschaukel, or "swing separator," has been previously described [26]. In the modified trennschaukel reported on here, composition as a function of time is measured in situ by thermistors (the composition difference at t = ∞ in the ends of the device being the separation

achieved). Previously, mass spectrometry was used exclusively, but in the present work it is used in several instances, primarily as a confirmatory technique. Wakeham [27] and Trengove et al. [28] have reported measurements of binary mixture composition in very accurately thermostated systems which are about an order of magnitude more precise than is possible with a mass spectrometer.

In the present work, the composition of binary gas mixtures is determined using thermistors (Keystone Carbon Company, L-904-75K-H-T2 and RL 10X04-10K-315-S5) of large negative temperature coefficient of resistance, typically three or four orders of magnitude for a temperature increase of 100 to 150 K. One arm of a Wheatstone bridge is a thermistor located in the unknown gas mixture, and another arm is a thermistor in a reference cell containing a binary mixture of the same gases at known composition. Sufficient current is passed for Joule heating of the thermistor in the unknown mixture, the temperature assumed by the thermistor, in part, being determined by the ability of the surrounding gas to dissipate heat via its thermal conductivity. Because the two thermistors are exposed to different gas mixtures, their temperatures (and hence their resistances) will differ, and the bridge becomes unbalanced. The bridge is calibrated so that the composition of the base mixture in the sensing cell is known in terms of the bridge imbalance. The reference thermistor is intended to compensate for fluctuations in both temperature and bridge voltage in the sample cell.

The top and bottom section thermistor gauges were calibrated separately with the entire device controlled at the upper or lower temperature by liquid cryogens and cold gases boiled off from the cryogens with reheat and control supplied by the associated electronics. Attainment of isothermality is the most difficult part of the experiment. The thermistors were calibrated over the composition range ∿45 to 55% He which is the nominal range of separation in the experiment.

The status of the experimental results at the time of the previous report [26] indicated that the results obtained by thermistor analysis were possibly somewhat low. This was indeed found to be the case from theoretical consideration which indicated excessive compression in the middle capillaries of the trennschaukel, due to too rapid pumping.

Furthermore, the composition measured by the thermistors did not agree well with the mass spectrometry analyses. The current techniques in pumping the trennschaukel and performing the calibrations have for the most part corrected these problems, as shown in Figure I-6 with additional experimental details given in Table I-5. The open circles show the previous results. The solid circles, experiments conducted where the pumping speed was low enough so that a viscous flow condition was realized and compression in the middle tubes was negligible, now agree quite well with the quantum curve, as well as with other work. These solid circles are α_T determined from the thermistor analysis (column 7 in Table I-5) and demonstrate better reproducibility and somewhat better agreement with the quantum theoretical calculation than α_T determined from mass spectrometry analyses. The next step in this work will be to determine α_T in the region between 30 and 82 K. Preparations are now being made for these experiments.

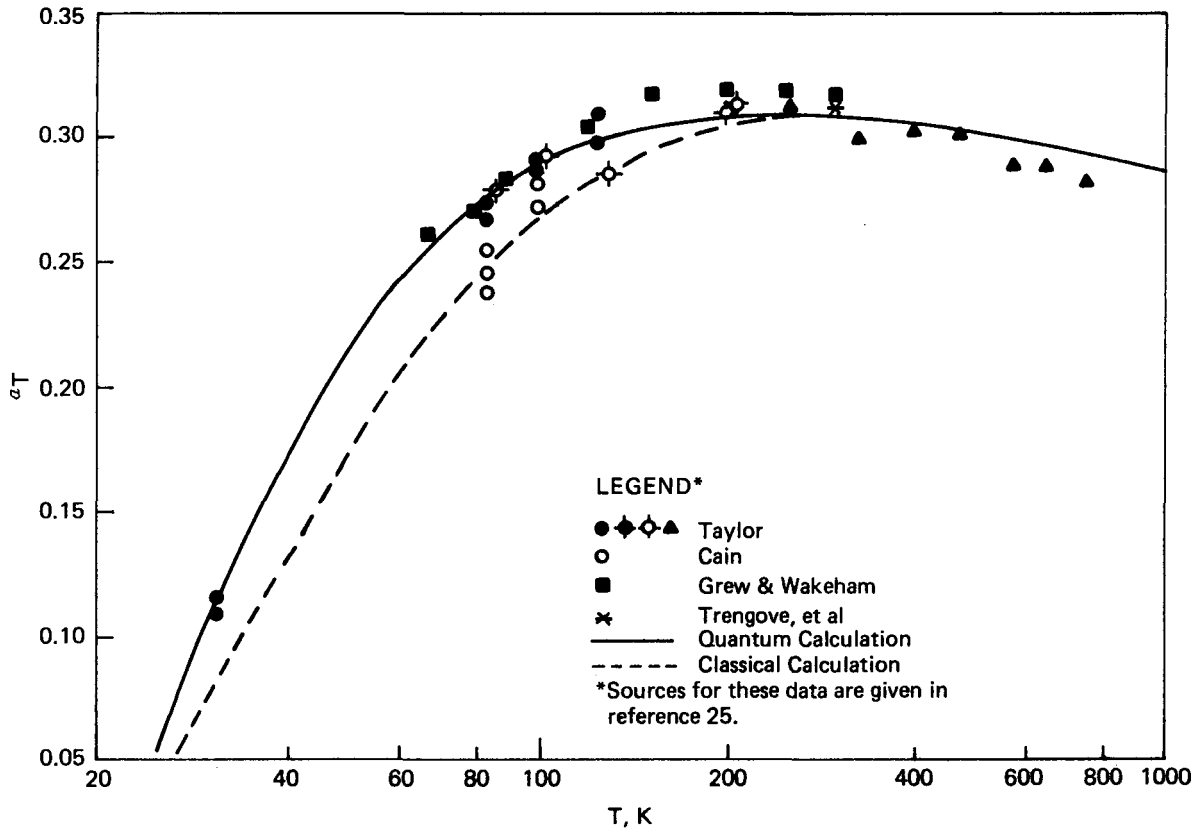

FIGURE I-6 - Thermal diffusion factor for equimolar ^{4}He-^{20}Ne.

Table I-5 - EXPERIMENTAL RESULTS

Exp No.	T_C (K)	T_H (K)	T_{AV} (K)	Feed Comp	P (torr)	α_T Thermistor Analysis	α_T Mass Spec Analysis
20	77	87	82	50/50	60	0.267	0.266
23	77	87	82	50/50	60	0.272	0.286
21	93	107	107	50/50	50	0.280	0.318
22	93	107	107	50/50	50	0.277	0.323
24	115	135	125	50/50	90	0.299	0.304
25	115	135	125	50/50	90	0.311	0.312

II. Separation research

Liquid phase thermal diffusion

W. M. Rutherford

Isotopic thermal diffusion data have been accumulated for a number of liquid compounds. It is appropriate at this time to examine the results for potential correlation of the thermal diffusion factor with molecular mass and structure. Although such a correlation may be empirical, it may provide essential information leading to a fundamental theoretical description of isotopic thermal diffusion in the liquid phase.

G. D. Rabinovich [1] suggested that the effect is dependent only on the molecular weights of the diffusing species with the result that the isotopic thermal diffusion factor is given by

$$\alpha_T = \alpha_o \frac{m_1-m_2}{m_1+m_2} \qquad (1)$$

where m is the molecular weight.

The limited data available to Rabinovich resulted in a value of 5.4 for α_o. Data acquired at this laboratory have generally resulted in much smaller values for α_o, and the results show clearly that α_o is by no means constant. For instance, significant differences have been found between the effects of ^{13}C and deuterium substitution in the same molecule [2]. Thus $\alpha_o = 4.8$ was found for benzene with the C_6D_6-C_6H_6 pair; whereas the corresponding value for the $^{13}C^{12}C_5$-$^{12}C_6H_6$ pair was 2.9. Similar effects have been found at this laboratory with isotopic substitutions in cyclohexane, chlorobenzene, and bromobenzene and by Ma and Beyerlein [3] in monodeuterated benzenes. Reichenbacher and Klemm [4] and Schirdewahn, Klemm, and Waldmann [5] have shown that the thermal diffusion factor in binary, isotopically substituted, gas phase hydrogen systems is represented within experimental accuracy by

$$\alpha_T = C_m(m_1-m_2)/(m_1+m_2) + C_I(I_1-I_2)/(I_1+I_2) \qquad (2)$$

where I is the second moment of the molecule. Equation (2) results from expansion of the thermal diffusion factor in a power series involving relative mass differences with the condition that

$$\alpha_{T12} = -\alpha_{T21} \qquad (3)$$

The coefficients of the series are dimensionless and independent of mass.

An equivalent relationship is postulated to apply to liquid phase systems. The first term of equation (2) incorporates the effect of mass differences between molecules, and the second is related to differences in the distribution of mass within the molecules. Thus equation (2) represents an extension of equation (1) to include structure as well as mass effects related to isotopic substitution.

As the basis for a preliminary evaluation of such a relationship, we examined the behavior of 6 binary systems involving isotopic substitutions in benzene, chlorobenzene, and bromobenzene. The systems and their corresponding isotopic thermal diffusion factors are listed in Table II-1.

The second moment of each molecule was calculated for an axis through the center of mass and perpendicular to the plane of

Table II-1 - ISOTOPIC THERMAL DIFFUSION FACTORS FOR SUBSTITUTED BENZENE SYSTEMS

System	α_T Measured	α_T Calculated
C_6H_6-C_6D_6	0.1650	0.1649
$^{13}C^{12}C_5H_6$-$^{12}C_6H_6$	0.0170	0.0178
$C_6H_5{}^{35}Cl$-$C_6H_5{}^{37}Cl$	0.0267	0.0282
$^{13}C^{12}C_5H_5{}^{35}Cl$-$^{12}C_6H_5{}^{35}Cl$	0.0117	0.0106
$C_6H_5{}^{35}Br$-$C_6H_5{}^{37}Br$	0.0173	0.0168
$^{13}C^{12}C_5H_5{}^{35}Br$-$^{12}C_6H_5{}^{35}Br$	0.0098	0.0082

the benzene ring. The reduced moment difference appearing in the second term of equation (2) was calculated therefrom. The data for the 6 systems were subsequently subjected to a linear regression analysis to determine the coefficients C_m and C_I, with the result that

$$\alpha_T = 1.973(m_1-m_2)/(m_1+m_2) + 0.973(I_1-I_2)/(I_1+I_2) \quad (4)$$

within a root mean square deviation of ±0.0013. This is on the order of the minimum estimated error in the measured values. The standard errors of estimate for the two coefficients were ±0.15 for C_m and ±0.062 for C_I. The mass parameter and the mass distribution parameter are both highly significant according to standard statistical criteria.

Figure II-1 is a plot of the measured thermal diffusion factor versus the thermal diffusion factor calculated from

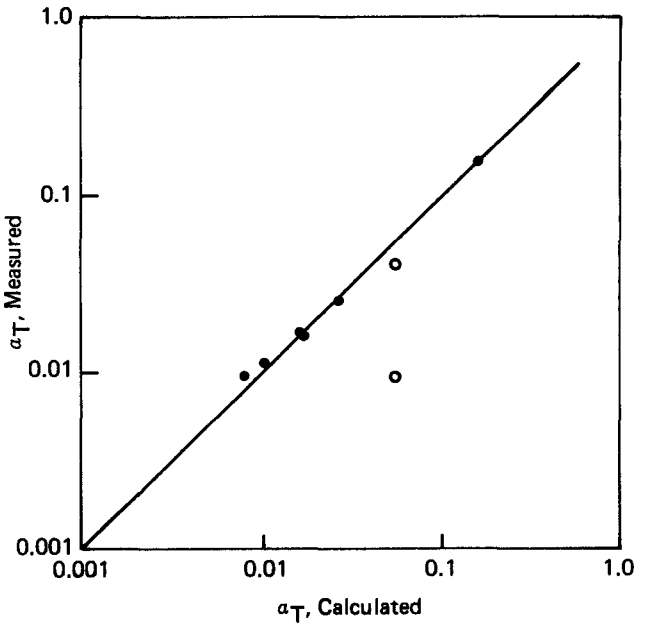

FIGURE II-1 - Measured versus calculated liquid phase isotopic thermal diffusion factors. The open circles are the measurements of Ma and Beyerlein for dideuterobenzene systems.

equation (4). Also plotted in Figure II-1 are the recent results of Ma and Beyerlein [3] for two systems involving ordinary benzene with 1,2 dideuterobenzene and 1,4 dideuterobenzene. The agreement is reasonably good with the single exception of the point for 1,2 dideuterobenzene. It seems reasonable to repeat the dideuterobenzene measurements at this laboratory, and preparations are being made to do this.

Calcium isotope separation

W. M. Rutherford

A process is being investigated for separating calcium isotopes by liquid phase thermal diffusion of an aqueous calcium nitrate solution. A technique was developed for selectively suppressing the separation of the salt from the water. The concept involves setting up a net

flow of water through the apparatus at a rate just sufficient to counteract separation of the solute from the solvent. According to theory previously developed [6], the separation of the isotopes is not affected by the solvent counterflow.

Work continued on the evaluation of modified columns. Two columns, which will be referred to as column A and column B, were tested. The columns are each 1.22 m long, but column A has a larger hot to cold wall spacing than does column B. Thus B would be expected to have a higher equilibrium separation factor than A. Conversely, A would be expected to have a somewhat higher transport rate than B. The hot and cold walls of the columns are made from nickel-200.

The experimental setup for the solvent counterflow process was described in an earlier report [7]. Solvent (water) is injected at a controlled rate into the bottom of the experimental column, and it is removed at the top by evaporation. The solvent injection rate is controlled by a laboratory computer to hold a constant solute concentration at the bottom of the column. The concentration is always controlled at a level somewhat higher than the top concentration in order to confer gravitational stability to the fluid column.

Two separate systems were used for the experiments. In the system for column B, a Mettler-Paar density meter was used to sense the bottom concentration. In the system for column A, a conductivity cell was used to perform the same function.

Five experiments were run with the two columns. The intent of the experiments was to assess the effect of two solute parameters, the top concentration and the concentration difference between bottom and top, on the isotopic separation. We were interested in getting high isotopic transport rates in column A; therefore, solute concentrations of 25% and higher were primarily of interest. In the case of column B, transport rate was not the major consideration; thus, lower solute concentrations were used.

Results of the experiments are given in Table II-2, along with the average values of the solute concentrations during the run. In Table II-2 the following definitions apply:

w_{st} = solute concentration at top, wt %

W_{sb} = solute concentration at bottom, wt %

$\ln q_{48}$ = natural logarithm of the ^{40}Ca-^{48}Ca separation factor.

Isotopic ratios are not yet available for the samples from run B2.

Upon disassembly of the columns at the conclusion of each run, solids were found deposited on the surfaces of the hot and cold walls at the bottom. The deposits were found to consist primarily of nickel salts. One would expect such deposits to occur from high pH solutions; therefore, pH measurements were routinely made after each run following the first observation of the deposits. The pH of the feed solutions is normally in the range 6.0 to 6.2. In every case (see Table II-2), we found that the pH had increased by several units throughout the system during the

Table II-2 - SEPARATION OF CALCIUM ISOTOPES BY LIQUID PHASE THERMAL DIFFUSION

Run	$\ln q_{48}$	w_{st}	w_{sb}	pH	
				Top	Bottom
Column A, nominal spacing 305 μm:					
1	0.44	24.8	32.8	-	-
2	-	25.0	30.5	8.5	10.9
3	0.31	35.6	40.6	9.0	10.7
Column B, nominal spacing 254 μm:					
1	0.38	25.5	35.0	9.2	11.2
2	0.53	6.0	10.9	9.0	10.7

run and that the pH at the bottom of the column was typically 2.1 to 2.7 units higher than the pH at the top.

Toward the end of the last run a brief attempt was made to reduce the pH by injecting 0.02 N nitric acid into the bottom of the column. The attempt was unsuccessful. Apparently the volume of deposited salts was already too large to be readily removed by a few milliequivalents of acid.

Solids deposited in the column are known to have a large adverse effect on column performance. The fact that such deposits regularly take place may explain some of the poor and erratic performance observed in these and earlier experiments. Isotopic separation data taken without counterflow in a 15-cm column suggest that much larger separations should be obtained in these longer columns; i.e., $\ln q_{48}$ approximately equal to 1 in column A and 2 in column B.

Our experience indicates that stainless steel is much more resistant to aqueous calcium nitrate than is nickel; hence, we are constructing a new stainless steel column for the next experiment. We have also procured a micro pH electrode so that we can measure, and perhaps control, the pH at the bottom of the column during the next experiments.

Zinc isotope separation

W. M. Rutherford

In previous work [8] we have found dimethyl zinc a suitable working fluid for the separation of zinc isotopes by liquid phase thermal diffusion. It was established that the pyrophoric fluid could be handled in a working system without undue hazard and without excessive degradation. Thermal diffusion column parameters for dimethyl zinc were subsequently evaluated in a specially built column 1.22-m long with a hot to cold wall working space of 254 μm.

Conceptual designs of practical scale isotope separation systems were developed based on the measured column parameters. The systems are multiple column cascades comprising assemblies of columns of various lengths and of various hot to cold wall spacings. The characteristics of such columns can be simply estimated with sufficient accuracy by the following:

$$H = H_r(a/a_r)^3 \quad (1)$$

$$Y = Y_r(a_r/a)^4(L/L_r) \quad (2)$$

where H is the initial transport coefficient, Y is the natural logarithm of the equilibrium separation factor, and the subscript r designates a reference column, the parameters of which are known.

A series of single cascades to enrich ^{68}Zn was calculated using the key weight method of de la Garza [9]. Product enrichments were in the range from 50 to 94% ^{68}Zn. The tails concentration was held constant at 10%, and the feed was the natural abundance composition given in Table II-3. The required cascade length, expressed in terms of Y, is plotted in Figure II-2. The length of the cascade increases rapidly as the product concentration goes above 90%. The shape of the curve is established by the abundances of the undesired isotopes. At the 50% level it is primarily ^{64}Zn that is being removed; whereas, at 80% ^{66}Zn is also being depleted and at 90%, ^{67}Zn. An effective upper limit for ^{68}Zn enrichment in a single cascade is established by the abundance of ^{70}Zn in the feed. A second cascade would be required to remove ^{70}Zn.

Table II-3 - NATURAL ABUNDANCES OF THE ZINC ISOTOPES

Isotope	Abundance (%)
^{64}Zn	48.89
^{66}Zn	27.81
^{67}Zn	4.11
^{68}Zn	18.57
^{70}Zn	0.62

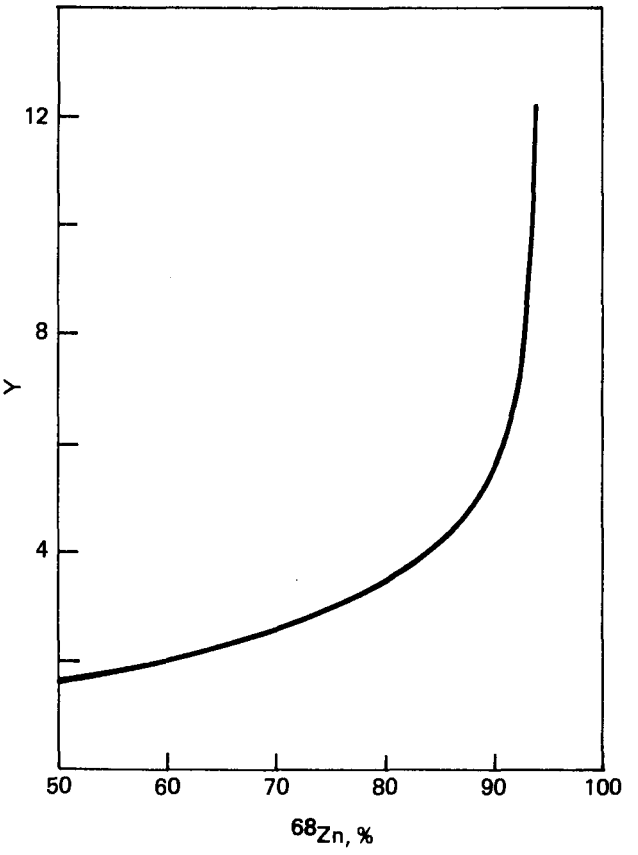

FIGURE II-2 - Dimensionless length of optimum key weight cascades for the separation of ^{68}Zn.

Figure II-3 is a plot of a typical cascade profile generated on the basis of the key weight concept. It represents the minimum separative power cascade for a key weight of 66.50 and a product concentration of 50%. The calculated profile is approximated by a squared-off cascade of 13 columns. The columns are of 3 types, designated A, B, and C in Table II-4.

Similar squared-off cascades were developed for product concentrations of 80 and 90%. The configurations of these cascades are given in Table II-5 along with production rates and composition of the products. A smaller, less efficient development cascade was also evaluated

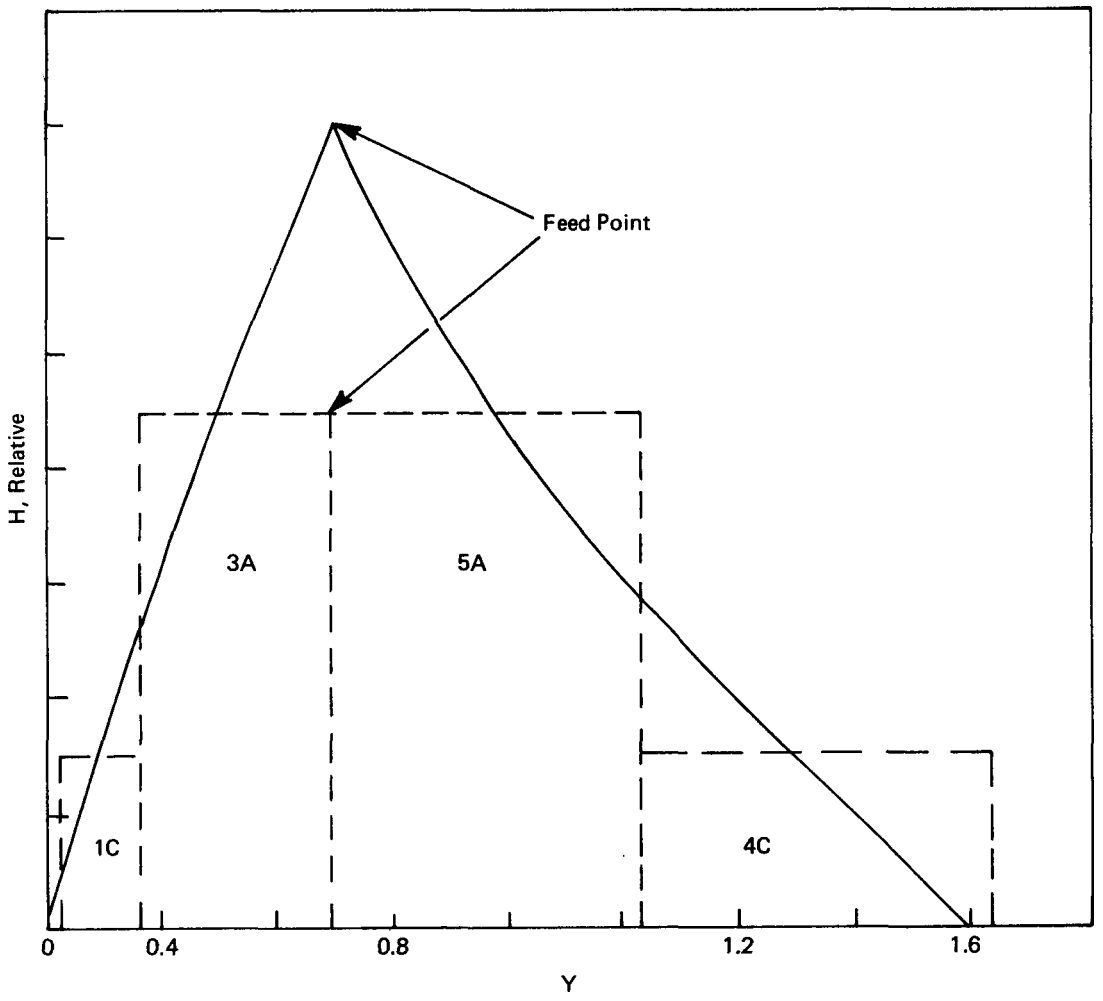

FIGURE II-3 - Cascade configuration for the separation of 50% ^{68}Zn. The solid line is the optimum key weight cascade. The dashed line is the squared off configuration given in Table II-3.

Table II-4 - THERMAL DIFFUSION COLUMN PARAMETERS FOR THE SEPARATION OF ZINC ISOTOPES USING DIMETHYL ZINC AS A WORKING FLUID

Column	Length (m)	Diameter (mm)	Spacing (μm)	$10^5 H^a$ (g/sec)	Y^a
A	2.44	25.4	330	5.00	0.106
B	1.22	25.4	254	2.28	0.152
C	1.22	19.1	254	1.71	0.152

[a] H and Y for one unit difference in isotopic mass.

Table II-5 - THERMAL DIFFUSION CASCADES FOR THE SEPARATION OF ZINC ISOTOPES

No. columns	11	13	27	39
Configuration[a]	3C/8C	1C-3A/5A-4C	2B-4A/8A-13C	2B-5A/8A-24C
Product conc, %	50	50	80	90
Product rate, g/yr ^{68}Zn[b]	185	439	312	247
Efficiency, %	74.4	90.7	88.3	88.7
Product Composition, %				
^{64}Zn	8.6	9.9	0.065	1.1×10^{-4}
^{66}Zn	31.2	30.0	8.2	0.64
^{67}Zn	7.9	7.7	7.4	4.1
^{68}Zn	50.0	50.0	80.0	90.0
^{70}Zn	2.3	2.4	4.4	5.3

[a]The columns are all in series; the slash denotes the feed point.

[b]Based on 300 days per year.

for producing 50% material. The results are also given in Table II-5.

The efficiencies listed in Table II-5 represent the ratio of the production rate of the squared-off cascade to that of an optimized key weight cascade of the same separative power.

Cascade performance during startup was calculated for the two 50% cascades. The desired product composition was reached after 30 days of operation in the large cascade and after 44 days of operation in the small cascade.

The results of these calculations show that it will be possible, but difficult, to produce considerable amounts of moderately enriched ^{68}Zn by liquid phase thermal diffusion.

Mutual diffusion

S. B. Wyrick and W. L. Taylor

Experiments to determine the mutual (or mass) diffusion coefficient of binary gas mixtures in the Hastelloy-X diffusion cell have been completed. The temperature range for this work has been approximately 350 to 1300 K. A new diffusion cell has been constructed of T-111 alloy, a mixture of tantalum/8% tungsten/2.4% hafnium. This cell, which is very similar to that used in the previous work [10-12], has been designed to operate in the temperature range of approximately 1000 to 2500 K. The highest temperatures achieved thus far for diffusion measurements have been about 1500 K.

The cell components have all been calibrated and assembled by electron beam welding. In order to operate at these

high temperatures a vacuum furnace is required to prevent oxidation of the cell. The vacuum furnace was acquired, modified, and installed, with its associated 40 kVA power supply, in place of the original Lindberg furnace. The diffusion cell is placed on a squat tripod inside a tungsten heating element which in turn is surrounded by several layers of tungsten radiation shielding. All of this is contained within a water-cooled copper can. Provision for temperature measurement is provided by a tungsten-rhenium thermocouple embedded in a slot milled in the side of the cell. The thermocouple and slot are covered by a T-111 radiation shield spot welded to the side of the cell. An optical line of sight has also been provided to the top of the cell for optical pyrometer observations. Access ports on the dome of the vacuum furnace have been installed to allow connection of bus bars for electrical power and feed lines (1/16-in. capillaries) to the cell. Feedthroughs into the vacuum region have also been provided for water cooling to the inner can, vacuum measurement, and temperature monitoring. The vacuum chamber has been leak checked and pumped down to 5×10^{-5} torr.

A system for analyzing the samples from the experiments has been prepared. Half of the samples will be analyzed by thermal conductivity and the other (redundant) half by mass spectrometer. The TC analyzer consists of a thermal conductivity cell, a constant temperature water bath and a manifold for controlling the flow of gases. The thermal conductivity cell is a cylindrical brass cell divided in half lengthwise. Each cell half contains a thermistor that is sensitive to the thermal conductivity of the gas in the cell. A reference gas is placed on one cell half while the gas to be analyzed is placed in the other cell half. Sapoff and Oppenheim [13] developed a method of analyzing the gases using the two previously mentioned thermistors in two arms of a Wheatstone bridge and resistors of fixed resistance in the remaining two arms. The bridge configuration is shown in Figure II-4.

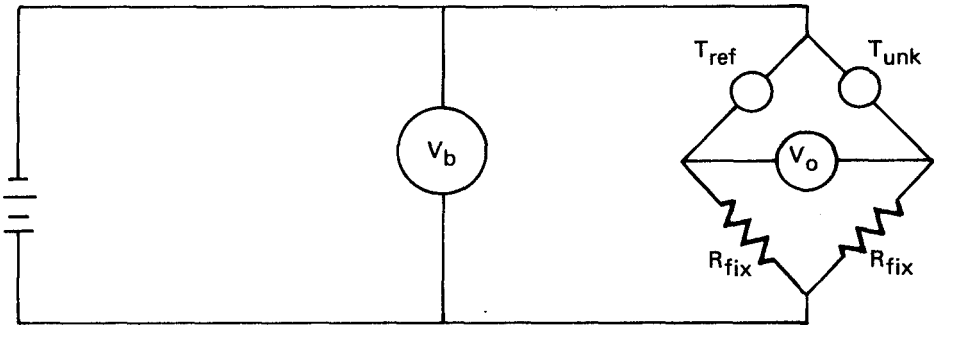

FIGURE II-4 - Wheatstone bridge configuration of TC analyzer. The components are: T_{ref}, thermistor in reference gas cell half; T_{unk}, thermistor in unknown gas cell half; R_{fix}, fixed resistors; V_b, voltage drop across circuit; and V_o, voltage drop difference of the thermistors.

V_b and R_{fix} are determined from E-I curves of the thermistors in the cell. Mixtures of known concentrations are used to provide a calibration curve and unknown mixtures can be determined from this curve. A slight drift problem has been observed in the analyzer.

When running the analyzer, V_o seemed to be changing at a constant rate. Further investigation showed that an E-I curve using the reference thermistor produced stable voltage drop readings, while an E-I curve using the unknown thermistor produced voltage drop readings which drift, indicating a possible leak in the unknown cell half. The cell was cleaned and sprayed with a leak sealant. No leak could be detected; however, a small drift persisted.

If the gas to be analyzed is introduced into the cell at a time t_0, the power for the bridge circuit turned on at time t_1 and the V_0 reading taken at time t_2, a reproducible calibration curve can be obtained if $t_1 - t_0$ and $t_2 - t_1$ are always held constant. The diffusion coefficients obtained from this analysis should be substantiated by those obtained from the mass spectrometer analysis.

Molecular beam scattering

R. W. York

SYSTEM MODIFICATIONS

The molecular beam chamber is nearing readiness for the continuation of total cross section experiments using the higher intensity beams possible with the installation of a high-throughput roots-type blower in the source exhaust chamber section.

Detector - The triple-pumped detector ion pumps and associated internal vacuum and electrical component connections were installed on the quadrupole detector system. The electronic connections from the detector and all other experimental chamber components were extended to their respective console locations in the new operational area locations. The detector housing was successfully vacuum tested on the chamber system. The vacuum chamber was then opened and the ionizer-quadrupole-multiplier unit was assembled and installed internally on the detector. All internal electrical connections were made, and the chamber was closed again for vacuum pumpdown.

An internal mirror, external cathetometer alignment system was installed to permit laser alignment of the beam-forming components in situ while the system is under vacuum. This alignment was previously made from laser alignment at atmospheric pressure using a calculated deflection when under vacuum. This method proved to be nonrepeating and, therefore, imprecise with no means for in situ correction.

Time-of-flight - The beam chopper was fitted with a new slotted disc designed for time-of-flight (TOF) measurements of the beam particle velocities. This should allow empirical determinations of beam velocity distributions for different beam species and operating conditions. The velocity distributions for the scattering experiments thus far performed have been "estimated" with a direct error effect on the final calculated experimental scattering cross section values. The addition of "measured" velocity distributions will, therefore, minimize this error contribution and permit a significant reduction in the overall experimental error. The TOF system has been installed in the vacuum system with all

internal instrument connections and aligned with the beam.

Target cell - The target gas cell used in total scattering cross section experiments is being modified to allow its controlled removal from the beam path and accurate replacement on the beam axis. This added capability will allow the unattenuated beam intensity to be measured between the experimental points when necessary to test for source intensity variations which might adversely affect the measured data.

The complete chamber system, with the exception of the target cell, is currently being vacuum leak checked and outgassed in preparation for resumption of total scattering cross section measurements and initial TOF measurements.

Zinc chemical exchange

B. E. Jepson

Zinc isotope exchange in two-phase liquid systems was investigated. Experimental equilibrium isotope effects for zinc have not been reported in the literature; however, a theoretical equilibrium separation factor (α) of 1.0007 per mass unit has been calculated for the $Zn(H_2O)_6^{2+}/ZnI_4^{2-}$ pair of complexes [14]. The same reference estimates a maximum possible separation factor of 1.00235 per mass unit for zinc isotope exchange and includes the basis for this calculation.

Separation factors of the magnitude of the aquo-iodo complex pair shown above are sufficiently large for possible application to zinc isotope enrichment by chemical exchange. In actual practice, a two-phase system separating these two complexes each into one phase cannot be devised; however, many other two-phase zinc systems can be devised with different zinc complexes.

Three general criteria must be present in a chemical exchange system for it to have practical applicability: (1) a two-phase liquid-liquid system into which different zinc species distribute at suitably large concentrations, (2) rapid exchange rate kinetics, and (3) a single stage separation factor (α) sufficiently large for a separations process.

TWO-PHASE SYSTEMS

In this work, three zinc two-phase systems were selected for study. The components of each of these systems are:

I. $TIBP/ZnCl_2/H_2O$

II. $DEHPA/ZnCl_2/CH_2Cl_2/H_2O$

III. $TIBP/ZnCl_2/cyclen/H_2O$

where: TIBP = Triisobutylphosphate

DEHPA = Di(2-ethylhexyl)phosphoric acid

cyclen = 1,4,7,10 tetraazacyclotetradecane

Some comments on aqueous zinc chloride solutions are pertinent. A 12.4 molar stock solution was prepared and diluted to the desired values. Zinc chloro complexes of the general formula $ZnCl_x^{2-x}$ tend to form in solutions. Zinc also undergoes hydrolysis in aqueous solutions according to the reaction:

$$ZnCl_2+H_2O \rightleftarrows Zn(OH)Cl_2^-+H^+ \qquad (1)$$

Measurements of pH, for example, were pH=4.4(2M0), pH=3.7(3M), pH=2.0(6M), and pH<0(12M). Because of the extremely high ionic strength, no conclusions were drawn

regarding the actual extent of hydrolysis. At concentrations around 0.5M, a precipitate of $Zn(OH)_2$ forms; however, above 1M no precipitate occurs. At very low concentrations, <<0.1M, at which the aquo zinc complex predominates, precipitates no longer occur; however, these concentrations are of no practical value to a chemical exchange process. Thus, at concentrations of interest, >1M, aqueous zinc solutions exist with a variety of coordination spheres and theoretical calculations such as that above represent hypothetical idealized situations.

System I is the simplest of the three studied. TIBP without diluent was used for the organic phase. It is a neutral extractant which extracts both zinc and its pair of chloride anions. Zinc concentrations used for the subsequent kinetics and separation factor work were 1.7M (aqueous) and 0.80M (organic). In System II, DEHPA functions as a liquid cation exchanger. Prior to equilibration of the two phases, a DEHPA methylene chloride solution was contacted repeatedly with concentrated $ZnCl_2$ solution, and the acidic aqueous solution was discarded. This was continued until a zinc concentration of 0.74M was attained in the organic phase. A high aqueous concentration was selected to ensure that zinc was present as the chloro complex. Concentrations used for the remaining work were 6.2M (aqueous) and 0.74M (organic). In System III, a water soluble crown compound was used to complex zinc. Cyclen (tetraaza 12 crown-4) was obtained as the tetrahydrochloride and reacted with a slurry of zinc oxide to neutralize the acid. Stoichiometric quantities of each compound were used; however, the reaction did not proceed to completion. Cyclen and ZnO did react in an approximately one to one ratio, and the excess zinc needed for extraction into the TIBP was supplied as aqueous $ZnCl_2$. Final zinc concentrations were 1.4M (aqueous) and 0.60M (organic). The amount of cyclen extracted into the TIBP was negligible.

EXCHANGE KINETICS

The heterogeneous exchange of zinc was studied in each system using stable zinc 68 as a tracer. The general procedure involved: (1) equilibration of the two phases, (2) separation of phases and labeling of the aqueous phase with zinc 68 solution, and (3) recontacting the two phases with vigorous mixing and sample removal as a function of time. In Systems I and III, the exchange had reached completion with 30 sec, the time of first sample withdrawal.

In System II, the exchange was only 60% complete in 30 sec, indicating the presence of a rate limitation. This limitation could be either a mass transfer limitation or a reaction rate limitation. These rates were considered to be sufficiently rapid for further study.

Isotope ratio measurements in the kinetics studies were obtained by neutron activation. The $^{68}Zn/^{64}Zn$ ratios could be directly determined because both the activated ^{69}Zn and ^{65}Zn can be counted. This method proved to be rapid and convenient for tracer studies that do not require a high degree of precision or accuracy.

SEPARATION FACTORS

Each of the three exchange systems was prepared with natural abundance zinc and mixed for a sufficient length of time to ensure that equilibrium was attained. Isotope ratio analyses of zinc samples

were carried out by mass spectrometry. Results of the isotopic analyses were inconclusive. For an element with several isotopes (e.g., Zn-64, 66, 67, 68) the consistency of isotope ratios between the phases can be evaluated by comparing the isotope effects for each ratio with that of the theoretical mass relationship.

The separation coefficient per mass unit for each pair of isotopes is given by the expression:

$$E_o = \frac{1}{\Delta M} \ln \frac{{}^{M_1}Zn \quad {}^{M_2}Zn \quad A}{{}^{M_1}Zn \quad {}^{M_2}Zn \quad B} \qquad (2)$$

where: E_o = separation coefficient

M_1, M_2 = masses of the isotope pair

$\Delta M = M_1 - M_2$ (>0)

A,B = aqueous and organic phases

The separation coefficients obtained for Systems I, II, and III were 0.0033 ± 0.0038, 0.0014 ± 0.0050, and 0.0031 ± 0.0031, respectively. The separation coefficients are on a per mass unit basis and the uncertainties are 95% confidence limits. It is evident that the precision of the measurements was insufficient to identify an isotope effect. Either improved isotope ratio analyses or multistage separations will be required to accomplish this.

Sulfur isotope enrichment via chemical exchange

W. K. Park and E. Michaels

CONCEPT

This work was initiated to establish, on a bench scale, an integral chemical exchange system complete with reflux units, for sulfur isotope enrichment. The major emphasis is placed on incorporating a bottom reflux unit into the overall system for self-sustained operation with minimum wastes. Operation of this system should provide a design basis for scaling-up to a pilot plant.

The reaction scheme selected for this work is based on isotope exchange between hydrogen sulfite ion, HSO_3^-, and SO_2 gas as follows:

$$H^{32}SO_3^- + {}^{34}SO_2 \rightleftarrows H^{34}SO_3^- + {}^{32}SO_2 \qquad (1)$$

Figure II-5 shows a schematic process flow diagram with $NaHSO_3$ solution as a process medium. The system consists of four sections: gas absorber, chemical exchanger, electrolyzer, and gas desorber. It is noted that the gas absorber is the top reflux unit for recycling SO_2, and the electrolyzer and gas-desorber combination is the bottom reflux unit for recycling SO_2 and also NaOH.

The major reactions that take place in each functional section of the system are:

Top reflux unit:

$$NaOH + SO_2 \rightarrow NaHSO_3$$
(in SO_2-absorber)

Chemical exchanger:

$$NaH^{32}SO_3 + {}^{34}SO_2 \rightleftarrows NaH^{34}SO_3 + {}^{32}SO_2$$
(in chemical exchanger)

Bottom reflux unit:

$$NaHSO_3 + H_2O \rightarrow NaOH + H_2SO_3$$
(in electrolyzer)

$$H_2SO_3 \rightarrow H_2O + SO_2$$
(in SO_2-desorber)

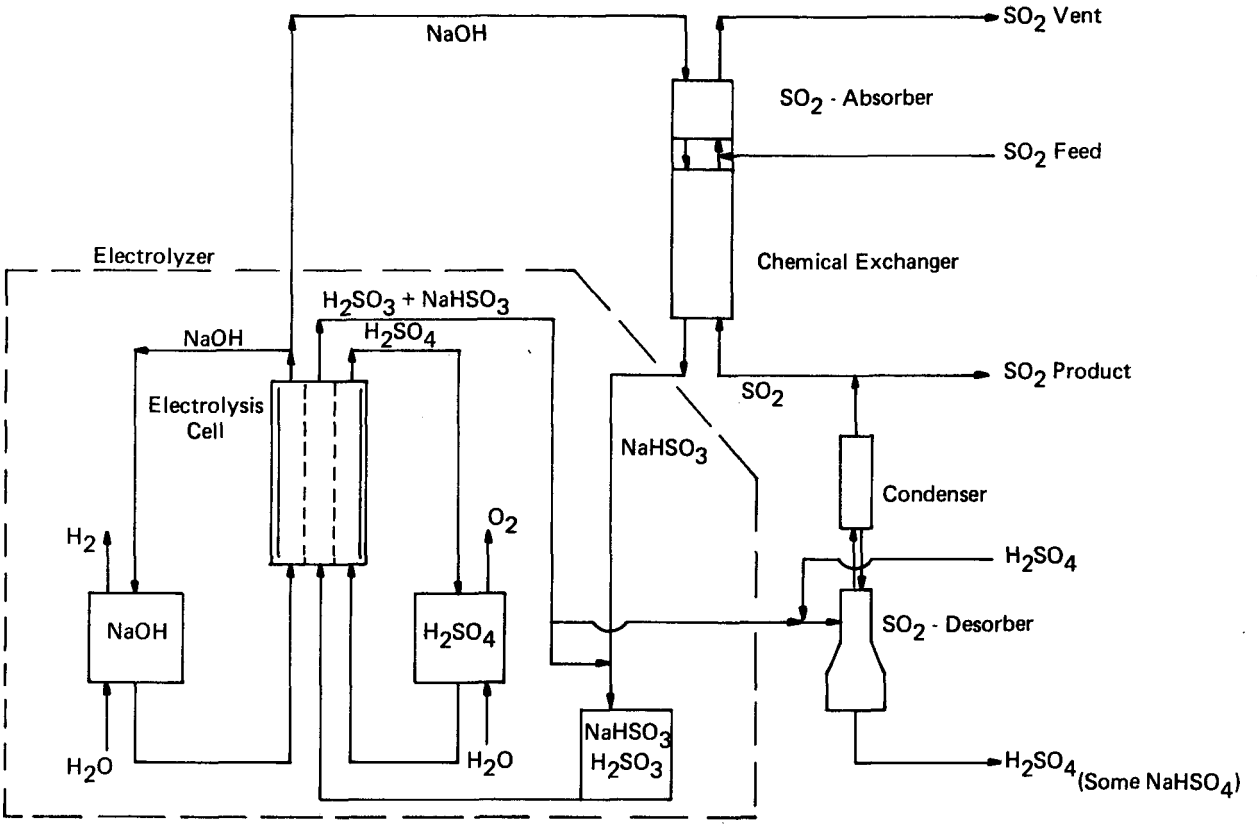

FIGURE II-5 - Process flow diagram for sulfur isotope enrichment system.

$$H_2{}^{34}SO_3 + H_2{}^{32}SO_4 \rightarrow H_2O + {}^{34}SO_2 + H_2{}^{32}SO_4$$
(in SO_2-desorber)

$$NaH^{34}SO_3 + H_2{}^{32}SO_4 \rightarrow H_2O + {}^{34}SO_2 + NaH^{32}SO_4$$
(in SO_2-desorber)

The scope of this work includes three tasks. The first task is to determine the technical feasibility of using an electrolysis system as a bottom reflux unit; the second task is to obtain an engineering data base with various operating conditions for overall process optimization; and the third task is to prepare a conceptual design for a pilot plant. This report covers the findings obtained from undertaking the first task.

ELECTROLYSIS TESTS

Various reflux units were conceptually studied as a means of recycling the process exit streams for closed-loop operation of the sulfur isotope chemical exchange system. A comparison of these units indicated that the membrane electrolysis unit with SO_2 desorber is technically most attractive, requiring relatively simple unit operations.

In this unit, positive ions can be selectively transferred from one solution through a membrane into another solution under a direct-current potential. Thus, the ion transfer and electrolytic reactions can take place continuously for

in-situ conversion and separation of the process exit stream into recycle streams.

Figure II-6 shows a schematic of the electrolytic conversion principle. The electrolysis cell consists of three compartments: (1) an anolyte compartment in which anode reactions take place continuously supplying H^+ ions to the feed stream through a cation membrane: (2) a feed compartment in which ion substitution reactions take place releasing Na^+ ions that are transferred to the catholyte solution through another cation membrane; (3) a catholyte compartment in which cathode reactions take place forming NaOH solution.

The principal reactions that proceed in the electrolysis cell are summarized below:

$$\tfrac{1}{2}H_2O \rightarrow \tfrac{1}{4}O_2 + H^+ + e^- \quad \text{(anolyte reaction)}$$

$$NaHSO_3 \rightarrow Na^+ + HSO_3^- \quad \text{(conversion reaction)}$$

$$H^+ + HSO_3^- \rightarrow H_2SO_3$$

$$H_2O + e^- \rightarrow OH^- + \tfrac{1}{2}H_2 \quad \text{(catholyte reaction)}$$

$$Na^+ + OH^- \rightarrow NaOH$$

The net result of this membrane electrolysis is continuous separation of the $NaHSO_3$ feed stream into HaOH and H_2SO_3 streams. The NaOH stream is recycled to

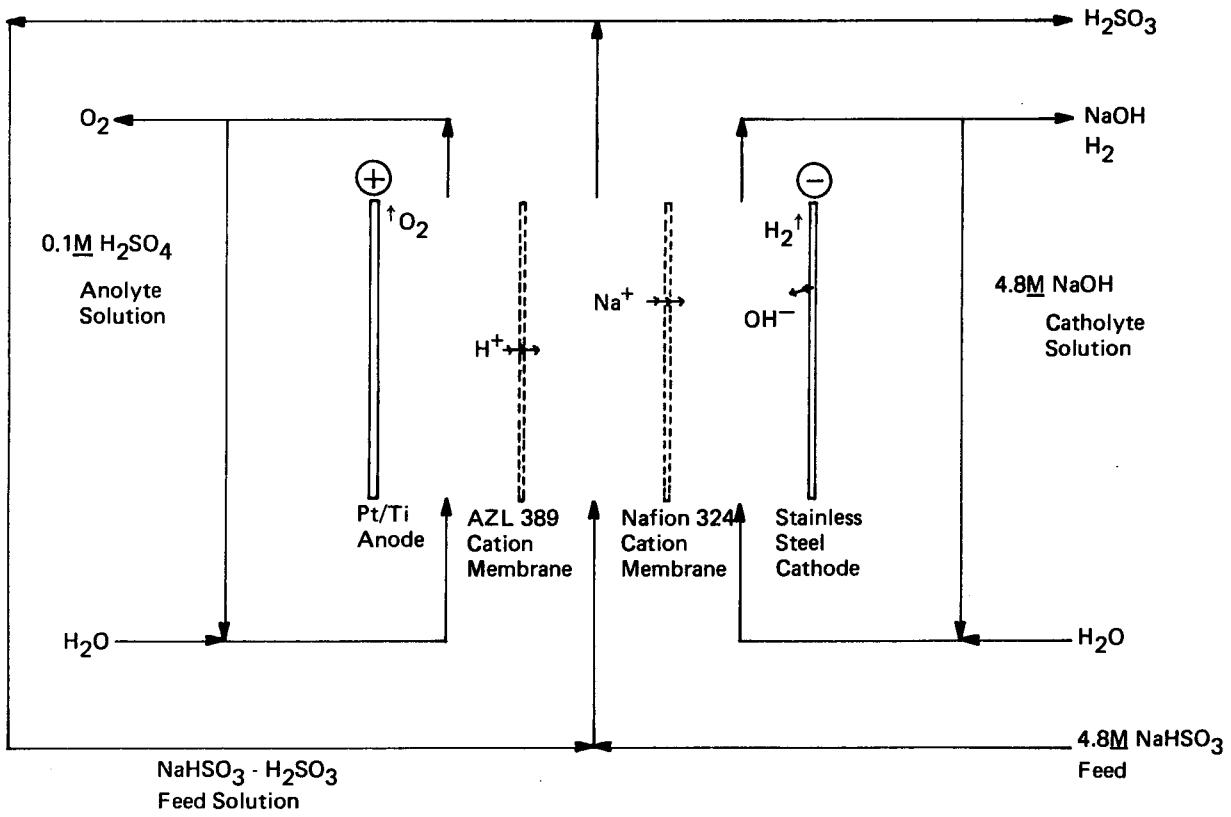

FIGURE II-6 - Schematic of electrolysis unit.

the gas absorber, and the H_2SO_3 stream is fed to the gas desorber for stripping SO_2 gas that is recycled to the chemical exchanger.

The electrolysis cell used for the feasibility testing is constructed of a Pt/Ti anode, an AZL 389 cation membrane, a Nafion 324 cation membrane, and a stainless steel cathode, as shown in Figure II-6. These cell components are structured in layers to form channels for fluid flow, and the whole assembly is held together with PVC and steel plates from both sides.

The experimental flow schematic is also reflected in Figure II-6. The simulated 4.8M $NaHSO_3$ feed solution was prepared by dissolving $NaHSO_3$ powder in deionized water. The anolyte solution was deionized water with 2% H_2SO_4 added to make it electrically conductive. The catholyte solution was 4.8M NaOH solution, and its concentration was held constant during the test run by continuously diluting with deionized water. The unit was operated in a batch mode. Starting with the holding tank provided for each stream, liquid in each stream passed through a pump, flow-rate regulating valve, rotameter, electrolysis compartment, and then back into the tank.

Samples of each stream were taken through a sample tap in the return line from the electrolysis cell. The hydraulics of all three streams were essentially identical as described above.

The electrolysis cell was energized by a DC power supply. A portion of this energy was dissipated into the solutions as heat, raising their temperatures to equilibrium levels (around 55°C).

Two runs were made with 4-L, 4.8M $NaHSO_3$ as a feed solution. For these runs a 4-L H_2SO_4 solution and a 2-L, 4.8M NaOH solution were used as the anolyte and catholyte solutions, respectively. The detailed operating conditions and their effects are listed in Table II-6. As the table indicates, the second run was made to confirm the results of the first, and to extrapolate the data points from 4 to 7½ hr electrolysis time.

Samples of the streams being processed through the electrolysis cell were collected at intervals (30 min or 1 hr) throughout the runs. These samples were than analyzed for pH, conductivity, and concentration. The sulfur content was analyzed using a total sulfur analyzer, and Na^+, HSO_3^-, SO_3^{2-}, and SO_4^{2-} ions were analyzed using an ion chromatograph.

The concentration change of the NaOH catholyte solution was monitored via titrations with a standard H_2SO_4 solution.

Current efficiency is the ratio of the number of equivalents removed per cell to the number of Faradays of electricity passed; that is,

$$e = F\,(N_1V_1 - N_2V_2) \,/\, (Ixt)$$

where
- e = efficiency
- N = solution normality
- F = Faraday's constant, 1608.3 A - min/equivalent
- V = Volume of batch, L
- (Ixt) = Amperes - minutes used
- sub 1 = conditions at start of run
- sub 2 = conditions at end of run

Up to 72% current efficiency was registered with a 182 mA/cm² current density.

Table II-6 - ELECTROLYSIS TEST CONDITIONS AND EFFECTS

Conditions	Run 1	Run 2
Feed solution	2L, 0.1M, H_2SO_4	3L, 0.1M, H_2SO_4
Anolyte solution	4L, 4.8M, $NaHSO_3$	4L, 4.8M, $NaHSO_3$
Catholyte solution	2L, 4.8M, NaOH	2L, 4.8M, NaOH
Anode side membrane	AZL 389	AZL 389
Cathode side membrane	Nafion 324	Nafion 324
Anode	Pt/Ti	Pt/Ti
Cathode	Stainless Steel	Stainless Steel
Electric potential, V	8 - 7	8 - 7
Current, A	40	40
Current density, mA/cm^2	182	182
Conductivity of feed, μs/cm	98,4000 - 96,100	98,400 - 64,900
Anolyte pressure, psi	3.7 - 5	5 - 3
Feed solution pressure, psi	3.3 - 5	5 - 3
Catholyte pressure, psi	3.5 - 5	5 - 3
Feed solution temperature, °C	25 - 58	25 - 54
Anolyte flow rate, L/min	1.6 - 1.4	2.0 - 1.3
Feed flow rate, L/min	2.0 - 2.5	2.5 - 1.3
Catholyte flow rate, L/min	1.6 - 1.8	2.0 - 1.5
pH of feed	4.3 - 2.5	4.3 - 2.3
Electrolysis time, hr	4	7½
Conversion, %	∿42	88
Current efficiency	0.66	0.72
Sulfur in catholyte, ppm	<200	<200

The rates of conversion were calculated on the basis of Na^+ ions transfer from the $NaHSO_3$ feed solution to the NaOH catholyte solution.

The conversion achieved in the first run was 42% in 4 hr of electrolysis time. The second run confirmed the first run results and demonstrated that the conversion rate remains nearly constant in time with the tested setting, achieving 88% conversion in 7½ hr of electrolysis.

In this feasibility testing, the material balance closure for sulfur was a critical factor because nearly 100% recycle of SO_2

must be achieved for efficient isotope enrichment. This factor raised two concerns: (1) the possible leak or transfer of sulfur from the feed stream through a membrane into other streams, and (2) the oxidation of H_2SO_3 into H_2SO_4.

In order to resolve the first concern, sulfur analysis on the NaOH catholyte solutions was conducted. The results showed no sulfur present in the catholyte solutions from both runs within the instrumental detection limit (<200 ppm). The second concern could not be resolved with the experimental set-up used for these runs. The liquid storage tanks for all three streams could not be sealed, thus allowing air into the system for extensive oxidation. A cursory evaluation of the data on SO_4^{2-} ion concentrations revealed that about 27% increase of SO_4^{2-} ion concentration occurred in the $NaHSO_3$ - H_2SO_3 feed stream in 4 hr of electrolysis. However, it appears that the oxidation can be minimized by using oxygen-purged solutions with some antioxidant in an air-tight system [15]. The next run to be made under such conditions will resolve this question.

In conclusion, the results obtained from the feasibility testing support the electrolytic reflux technique as a viable method for converting sodium bisulfite into sodium hydroxide and sulfurous acid.

References

I. Low temperature research

1. Mound Activities in Chemical and Physical Research: January-June 1982, MLM-2998, Monsanto Research Corporation, Miamisburg, Ohio, October 1982, pp. 15-16.

2. Mound Activities in Chemical and Physical Research: July-December 1982, MLM-3072, Monsanto Research Corporation, Miamisburg, Ohio, June 1983, pp. 8-10.

3. Hiskes, J. R., M. Bacal, G. W. Hamilton, Lawrence Livermore National Laboratory Report No. UCID-18031 (unpublished), 1979.

4. Estimated from H_2 and D_2 results, M. Allan and S. F. Wong, Phys. Rev. Lett., 41, 1791 (1978).

5. Barnet, C. F., et al, ORNL-5206 and ORNL-5207, Oak Ridge National Laboratory, Oak Ridge, Tennessee, February 1977.

6. Papagiannakopoulos, P. J. and C. E. Easterly, ORNL/TM-6699, Oak Ridge National Laboratory, Oak Ridge, Tennessee, May 1979.

7. Chupka, W. A., et al., J. Chem. Phys., 48, 1518 (1968).

8. Burt, J. A., et al., J. Chem. Phys., 52, 6062 (1970).

9 Bacal, M. and G. W. Hamilton, Phys. Rev. Lett., 42, 1538 (1979).

10. Hiskes, J. R., A. M. Karo, M. Bacal, A. M. Bruneteau, and W. G. Graham, J. Appl. Phys., 53, 3469 (1982).

11. Souers, P. C., E. M. Fearon, and R. T. Tsugawa, to be published.

12. Aguilanti, V., A. Galli, A. Giardini-Guidoni, G. G. Volpi, J. Chem. Phys., 43, 1969 (1965).

13. Douglass, C. H., G. Ringer, and W. R. Gentry, J. Chem. Phys., 76, 2423, (1982).

14. Mound Activities in Chemical and Physical Research: July-December 1983, MLM-3150, Monsanto Research Corporation, Miamisburg, Ohio, June 1984, pp. 10-11.

15. Berry, K. H., Temperature, Its Measurement and Control in Science and Industry, James F. Schooley, ed., APS 1983, pp. 21-24.

16. Gammon, B. E., J. Chem. Phys., 64, 2556 (1976).

17. Briggs, T. C., Bureau of Mines Report of Inv. 7352, March 1970.

18. Guildner, L. A. and R. E. Edsinger, J. Res. NBS 80A, 716 (1976).

19. Feltgren, R., J. Chem. Phys., 76, 2360 (1982).

20. Feltgren, R., J. Chem. Phys., 74, 1186 (1981).

21. Ahlrichs, R., R. Penco, and G. Scoles, Chem. Phys., 19, 119 (1970).

22. Plumb, H. H., Temperature, Its Measurement and Control in Science and Industry, James F. Schooley, ed., APS 1983, pp. 77-88.

23. Gugan, D., Metrologia, 19, 147 (1984).

24. Liu, B., and A. D. McLean, J. Chem. Phys., 59, 4557 (1973).

25. Unpublished calculations (1975) cited in J. A. Barker and D. Henderson, Rev. Mod. Phys., 48, 587 (1976).

26. Mound Activities in Chemical and Physical Research: January-June 1983, MLM-3125, Monsanto Research Corporation, Miamisburg, Ohio, December 1983, p. 6.

27. Wakeham, W. A., J. Phys. E: Sci Instrum, 4, 443 (1971).

28. Trengove, R. D., H. L. Robjohns, T. N. Bell, M. L. Martin, and P. J. Dunlop, Physica, 108A, 488 (1981).

II. Separation research

1. Rabinovich, G. D., Inzh.-Fiz. Zh., 15, 1014 (1968).

2. Rutherford, W. M., J. Chem. Phys., 59, 6061 (1973).

3. Ma, N. R. and A. L. Beyerlein, J. Chem. Phys., 78, 7010 (1983).

4. Reichenbacher, W. and A. Klemm, Z. Naturforsch., 19a, 1051 (1964).

5. Schirdewahm, J., A. Klemm, and L. Waldmann, Z. Naturforsch., 16a, 133 (1960).

6. Rutherford, W. M. and K. W. Laughlin, Science, 211, 1054 (1981).

7. Mound Activities in Chemical and Physical Research: July-December 1981, MLM-2892, Monsanto Research Corporation, Miamisburg, Ohio, May 1982, p. 18.

8. Mound Activities in Chemical and Physical Research: July-December 1983, MLM-3150, Monsanto Research Corporation, Miamisburg, Ohio, June 1984, p. 14.

9. de la Garza, A., Chem. Engr. Science, 18, 73 (1963).

10. Cain, D. and W. L. Taylor, J. Chem. Phys., 71, 3601 (1979).

11. Taylor, W. L. and D. Cain, J. Chem. Phys., 78, 6220 (1983).

12. Taylor, W. L. and D. Cain, High Temp. - High Press., 15, 433 (1983).

13. Sapoff, M. and R. M. Oppenheim, Proc. IEEE, 51, 1292 (1963).

14. Zhavoronkov, N. M., D. A. Knyazev, A. A. Ivlev, and G. D. Klinski, Russian Chemical Review, 49, (3) (1980), pp. 203-221.

15. Andreev, B. M. and A. S. Polevoi, Russian Chemical Review, 52, 213-228 (1983).

Distribution

EXTERNAL

TIC-4500, UC-4 and UC-22 (194)

J. R. Blair, DOE/Office of Health and Environmental Research

J. Burnett, DOE/Office of Basic Energy Sciences

J. S. Cantrell, Miami University, Oxford, Ohio

G. R. Gartrell, DOE/Dayton Area Office

K. Gschneider, Iowa University, Ames, Iowa

N. Haberman, DOE/Division of Nuclear Energy

H. N Hill, DOE/Dayton Area Office

J. N. Maddox, DOE/Office of Health and Environmental Research

L. R. Morss, Argonne National Laboratory

H. A. Schneiderman, Monsanto, St. Louis

F. D. Stevenson, DOE/Office of Basic Energy Sciences

L. Thompson, University of Minnesota

E. L. Venturini, Sandia National Laboratories, Albuquerque

D. White, University of Pennsylvania

Monsanto Reports Library, R2C, St. Louis

INTERNAL

G. C. Abell

W. R. Amos

C. T. Bishop

R. C. Bowman

D. Cain

D. G. Carfagno

V. R. Casella

R. E. Ellefson

B. M. Farmer

H. N. Friedlander

C. S. Friedman

W. B. Hogeman

C. W. Huntington

B. E. Jepson

B. R. Kokenge

G. T. McConville

D. A. Menke

E. D. Michaels

R. H. Nimitz

W. K. Park

W. M. Rutherford

W. E. Sheehan

G. C. Shockey

G. L. Silver

W. L. Taylor

R. J. Tomasoski

R. E. Vallee

C. J. Wiedenheft

W. R. Wilkes

S. B. Wyrick

R. W. York

Document Control

Library (15)

Publications

Published by Information Services:
Stephen L. Nowka, Editor